*Appl. Math. Mech. -Engl. Ed.*, **43**(3), 355–370 (2022)

**APPLIED MATHEMATICS AND MECHANICS (ENGLISH EDITION)**

https://doi.org/10.1007/s10483-022-2828-5

# Buckling analysis of functionally graded nanobeams under non-uniform temperature using stress-driven nonlocal elasticity*

Chi XU[1,2], Yang LI[1,2], Mingyue LU[2], Zhendong DAI[1,2,†]

1. College of Mechanical and Electrical Engineering, Nanjing University of Aeronautics and Astronautics, Nanjing 210016, China;
2. Jiangsu Provincial Key Laboratory of Bionic Functional Materials, Nanjing University of Aeronautics and Astronautics, Nanjing 210016, China

(Received Sept. 8, 2021 / Revised Dec. 20, 2021)

**Abstract** In this work, the size-dependent buckling of functionally graded (FG) Bernoulli-Euler beams under non-uniform temperature is analyzed based on the stress-driven nonlocal elasticity and nonlocal heat conduction. By utilizing the variational principle of virtual work, the governing equations and the associated standard boundary conditions are systematically extracted, and the thermal effect, equivalent to the induced thermal load, is explicitly assessed by using the nonlocal heat conduction law. The stress-driven constitutive integral equation is equivalently transformed into a differential form with two non-standard constitutive boundary conditions. By employing the eigenvalue method, the critical buckling loads of the beams with different boundary conditions are obtained. The numerically predicted results reveal that the growth of the nonlocal parameter leads to a consistently strengthening effect on the dimensionless critical buckling loads for all boundary cases. Additionally, the effects of the influential factors pertinent to the nonlocal heat conduction on the buckling behavior are carefully examined.

**Key words** size effect, stress-driven nonlocal model, constitutive boundary condition, nonlocal heat conduction, functionally graded (FG) beam, buckling load

**Chinese Library Classification** O342
**2010 Mathematics Subject Classification** 74K10

## 1 Introduction

Beam-like nanostructures, as the most common elements, have a wide range of applications in nanodevices, such as gecko's nano-adhesive setae[1], self-assembled DNA nanostructures[2], single nanometer zinc oxide columns of nanofriction generators[3], and one-dimensional van der Waals heterostructures made from boron nitride and single-walled carbon nanotubes[4]. With the development of more advanced equipment and approaches for preparing high-performance

* Citation: XU, C., LI, Y., LU, M. Y., and DAI, Z. D. Buckling analysis of functionally graded nanobeams under non-uniform temperature using stress-driven nonlocal elasticity. *Applied Mathematics and Mechanics* (*English Edition*), **43**(3), 355–370 (2022) https://doi.org/10.1007/s10483-022-2828-5

† Corresponding author, E-mail: zddai@nuaa.edu.cn

Project supported by the National Natural Science Foundation of China (Nos. 51435008 and 51705247) and the China Postdoctoral Science Foundation (No. 2020M671474)

materials (e.g., laser-assisted electrochemical growth of micro-nano metal rods, ultraviolet, and magnetic particle-assisted polymer curing), the concept of functionally graded (FG) design has also been introduced to the nanostructures[5–6]. Due to the extraordinary photoelectric-thermo-mechanical properties, the topics associated with FG nanobeams have been of particular interest to the interdisciplinary scientific community.

It is known that when the size of a material alters from macro to micro, its mechanical properties dramatically change, owing to the so-called size effect. This effect is supported by many experiments and simulations[7–9]. For such structural problems, the classical continuum mechanics is invalid, since it does not contain any scale parameters[10–12]. On the other hand, first-principle calculation and molecular dynamics simulation usually require a large amount of computational resources. For these reasons, studying the mechanical response of nanostructures via non-classical continuum-based theories has become a topic of significance in the literature.

Among the non-classical continuum mechanics, Eringen's nonlocal elasticity theory is one of the most popular models. Eringen assumed that the stress field at the reference point can be expressed as a convolution integral of an attenuating kernel function and strains within the entire spatial domain. Further, a characteristic scale parameter is considered to evaluate the intensity of the size effect[13–15]. In recent years, Eringen's nonlocal model has been widely implemented to examine various static and dynamic problems of nanobeam structures, such as static bending, free vibration, and buckling. Ghannadpour et al.[16] performed elastic buckling and flexural analyses of nonlocal Bernoulli-Euler beams by utilizing the Ritz method. Khodabakhshi and Reddy[17] established a finite-element-based model based on the two-phase integro-differential form of Eringen's nonlocal elasticity model to scrutinize the static bending behavior of Bernoulli-Euler beams. Sobhy and Zenkour[18] inspected the influence of the magnetic field on the thermo-vibro-buckling behavior of viscoelastic sandwich-like nanobeams accounting for their viscoelasticity. Lu et al.[19] explored the simultaneous effects of the nonlocal stress and strain gradient on the buckling behavior of nanobeams. Based on Eringen's nonlocal elasticity theory, Mirjavadi et al.[20] examined the buckling and free vibrational behaviors of axially FG nanobeams accounting for the thermal effect. Barati and Zenkour[21] reported the post-buckling behavior of general higher-order FG nanobeams with porosity distributions. By employing the nonlocal strain gradient theory, Al-Shujairi and Mollamahmutoglu[22] assessed the linear buckling and transverse vibration of size-dependent sandwich-like FG microbeams with thermal effects. In these studies, Eringen's nonlocal elasticity theory can suitably explain well parts of the mechanical behavior and has a consistent softening effect[23–25].

However, it has recently been proved that Eringen's nonlocal model is ill-posed for some bounded structures. Two constitutive conditions are not considered during transforming from the nonlocal integral-based model to the differential-based one[26–28]. In some specific cases, these two constitutive boundary conditions conflict with the equilibrium requirements of the problem. To overcome this deficiency, Romano and Barretta[29] established a novel stress-driven nonlocal elasticity theory, by which the conflict between the boundary conditions was eliminated[30–32]. Based on this novel theory, many mechanical responses of micro-nano structures have been scrutinized in the past few years[33–36].

In addition to the advanced elasticity theory of nanoscale solid, the size effect of heat conduction has also attracted much attention, since many studies have pointed out that the heat conduction at micro-/nano-size would be inherently nonlocal. In other words, the characteristic length of the material should be appropriately introduced to the constitutive relation of the heat flux to improve the classic heat conduction law[37–38]. To this end, Yu et al.[39–40] proposed a nonlocal thermo-elasticity-based model, in which the nonlocal characteristics of both elastic body and heat conduction were incorporated into the governing equation. Based on that suggested model, Yu et al.[41] evaluated the critical buckling loads of Bernoulli-Euler beams. Lei et al.[42] studied the effect of nonlocal thermoelasticity on buckling response of axially FG nanobeams. Barati and Zenkour[43] discussed the forced vibration, bending, and buckling anal-

ysis of FG nanobeams, resting on elastic foundations in hygro-thermal environments. Although the size dependency of heat transfer has been involved in the above-mentioned studies, yet their corresponding formulations were fully organized based on Eringen's nonlocal model[44–45]. As mentioned earlier, such a model would not be suitable for the analysis of bounded nanostructures.

In the present work, by combining the nonlocal heat transfer and the well-posed stress-driven nonlocal elastic model, we develop a novel nonlocal thermo-elastic model for buckling analysis of the FG Bernoulli-Euler beam in a non-uniformly thermal environment. The governing equations and their associated corresponding boundary conditions are deduced from the variational principle of virtual work. Two constitutive boundary conditions are taken into account to meet the requirements of full equivalence between the stress-driven nonlocal constitutive integral equations and their corresponding differential ones, and then an exact solution for the critical buckling loads of the FG beam is obtained. In numerical simulations, the effects of functionally gradient index, as well as nonlocal factors pertinent to the stress and heat conduction, on the buckling behavior are examined and discussed in some detail.

## 2 Problem formulations

### 2.1 FG Bernoulli-Euler nanobeam model

Consider an FG straight nanobeam whose length, width, and thickness in order are represented by $L$, $b$, and $h$. The coordinate system is demonstrated in Fig. 1. Young's modulus of the FG nanobeam is symmetrical about the mid-plane and varies smoothly from the middle to the sides of the beam by the following power-law[46–47]:

$$E(z) = (E_{\mathrm{H}} - E_{\mathrm{L}})\, V_{\mathrm{H}}(z) + E_{\mathrm{L}}, \tag{1}$$

where

$$V_{\mathrm{H}}(z) = \begin{cases} \left(\dfrac{z-h_0}{h_1-h_0}\right)^{\alpha}, & h_0 \leqslant z < h_1, \\ \left(\dfrac{z-h_2}{h_1-h_2}\right)^{\alpha}, & h_1 \leqslant z \leqslant h_2, \end{cases} \tag{2}$$

in which $E_{\mathrm{H}}$ and $E_{\mathrm{L}}$ indicate Young's modulus of constituent materials, $h_1$ is located at the mid-plane, and the mid-plane is taken as the $Oxy$-plane[48–49]. Figure 2 presents the variation of Young's modulus $E(z)$ through the thickness of the FG nanobeam for various power-law indexes $\alpha$.

In the framework of the Bernoulli-Euler beam theory, the displacement field is defined as

$$u_x = -zw', \quad u_y = 0, \quad u_z = w. \tag{3}$$

The normal elastic strain $\varepsilon_{xx}$ is given as

$$\varepsilon_{xx} = -zw''. \tag{4}$$

According to the variational principle of virtual work, the relationship between the variation of the virtual strain energy $\delta U$ and the total potential of the external load $\delta W$ can be given as

$$\delta U - \delta W = M'\delta w\big|_0^L - M\delta w'\big|_0^L - N_{\mathrm{a}}w'\delta w\big|_0^L + \int_0^L (N_{\mathrm{a}}w'' - M'')\,\delta w \,\mathrm{d}x = 0, \tag{5}$$

in which the axial compressive force $N_{\mathrm{a}}$ and the bending moment $M$ are defined respectively as

$$\begin{cases} N_{\mathrm{a}} = N_{\mathrm{T}} + N_{\mathrm{M}} = \displaystyle\int_A \sigma_{xx}\,\mathrm{d}A, \\ M = \displaystyle\int_A z\sigma_{xx}\,\mathrm{d}A, \end{cases} \tag{6}$$

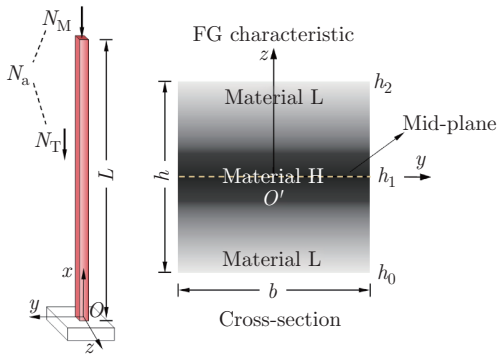


**Fig. 1** Schematic representation of the FG Bernoulli-Euler nanobeam with axial mechanical and thermal loads (red color represents the temperature distribution, while the grey color on the cross-section indicates the varying Young's modulus) (color online)

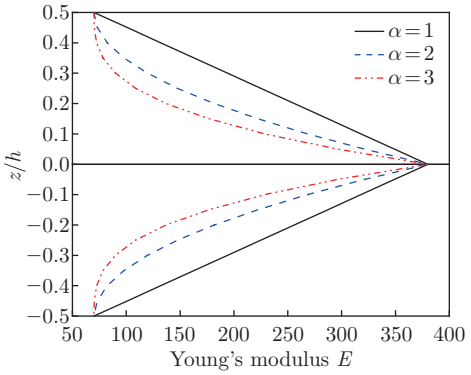


**Fig. 2** Variation of Young's modulus $E$ of the FG nanobeam across the thickness for various values of the power-law index $\alpha$ ($E_L = 70$ GPa, and $E_H = 380$ GPa) (color online)

where $N_T$ denotes the axial thermal force produced by the non-uniform temperature field, and $N_M$ represents the axial mechanical force. $A$ is the cross-sectional area of the beam.

From Eq. (5), the equilibrium equation of the problem can be obtained as follows:

$$N_a w'' - M'' = 0, \tag{7}$$

and the standard boundary conditions are

$$\begin{cases} (M' - N_a w')\delta w|_0^L = 0, \\ M\delta w'|_0^L = 0. \end{cases} \tag{8}$$

### 2.2 Stress-driven nonlocal elastic model

Based on the stress-driven nonlocal integral formulation presented in Refs. [26] and [30], the constitutive relation of the FG straight nanobeam defined in the integral form within the spatial domain can be given as

$$\int_0^L \psi\left(|x - x'|, \xi\right) \sigma_{xx}\left(x'\right) \mathrm{d}x' = E\varepsilon_{xx}(x) = -Ezw'' - E\alpha_\theta\theta, \tag{9}$$

where $\sigma_{xx}$ denotes the nonlocal axial stress. The kernel function $\psi\left(|x - x'|, \xi\right)$ depends on the Euclidean distance. $\xi$ represents the nonlocal elastic parameter. $\alpha_\theta$ is the coefficient of thermal expansion, and $\theta$ is the temperature change.

In the present study, adopting a bi-exponential kernel function is set as follows[30]:

$$\begin{cases} \psi = \dfrac{1}{2\kappa} \mathrm{e}^{-\frac{|x-x'|}{\kappa}}, \\ \kappa = \xi L, \end{cases} \tag{10}$$

where $\kappa$ is a length-scale parameter.

By Eq. (9), the constitutive equation for the buckling is expressed as

$$-E(z)zw'' = \frac{1}{2\kappa} \int_0^L \mathrm{e}^{-\frac{|x-x'|}{\kappa}} \sigma_{xx} \, \mathrm{d}x'. \tag{11}$$

On the basis of the definition of $M$ in Eq. (6), it can be given as

$$\begin{cases} -A_2 w'' = \dfrac{1}{2\kappa}\displaystyle\int_0^L \mathrm{e}^{-\frac{|x-x'|}{\kappa}} M \,\mathrm{d}x', \\ A_2 = \displaystyle\int_A z^2 \cdot E(z)\mathrm{d}A. \end{cases} \tag{12}$$

According to the given calculations in Appendix A, Eq. (12) would be equivalent to the following differential form:

$$\frac{1}{\kappa^2}(-A_2 w'') - (-A_2 w^{(4)}) = \frac{1}{\kappa^2} M \tag{13}$$

with two constitutive boundary conditions

$$\begin{cases} (-A_2 w'''(0)) - \Big( -\dfrac{1}{\kappa} A_2 w''(0)\Big) = 0, \\ (-A_2 w'''(L)) + \Big( -\dfrac{1}{\kappa} A_2 w''(L)\Big) = 0. \end{cases} \tag{14}$$

By substituting Eq. (13) into Eq. (7), a sixth-order ordinary differential equation is derived for the static buckling behavior in the framework of nonlocal elasticity as

$$\kappa^2 A_2 w^{(6)} - A_2 w^{(4)} - N_{\mathrm{a}} w'' = 0. \tag{15}$$

For the case of $\kappa = 0$, Eq. (15) can be degraded to the classical model of buckling.

The general solution to this standard equation can be assumed as

$$\begin{aligned} w(x) = &-2D\Big(\frac{\mathrm{e}^{x\sqrt{-D_1/D}/\sqrt{2}}}{D_1} C_1 + \frac{\mathrm{e}^{-x\sqrt{-D_1/D}/\sqrt{2}}}{D_1} C_2 - \frac{\mathrm{e}^{x\sqrt{D_2/D}/\sqrt{2}}}{D_2} C_3 - \frac{\mathrm{e}^{-x\sqrt{D_2/D}/\sqrt{2}}}{D_2} C_4\Big) \\ &+ xC_5 + C_6, \end{aligned} \tag{16}$$

where $D = \kappa^2\sqrt{A_2}$, $D_1 = -\sqrt{A_2} + \sqrt{A_2 + 4N_{\mathrm{a}}x^2}$, $D_2 = \sqrt{A_2} + \sqrt{A_2 + 4N_{\mathrm{a}}x^2}$, and $C_i$ are unknown coefficients.

We consider four types of boundary edges, i.e., clamped-clamped (CC), clamped-simply supported (CS), simply supported-simply supported (SS), and clamped-free (CF). The corresponding standard conditions can be written as

$$\begin{cases} \text{CC}: & w(0) = 0, & w'(0) = 0, & w(L) = 0, & w'(L) = 0, \\ \text{CS}: & w(0) = 0, & w'(0) = 0, & w(L) = 0, & M(L) = 0, \\ \text{SS}: & w(0) = 0, & M(0) = 0, & w(L) = 0, & M(L) = 0, \\ \text{CF}: & w(0) = 0, & w'(0) = 0, & M(L) = 0, & M'(L) - N_{\mathrm{a}} w'(L) = 0. \end{cases} \tag{17}$$

Using these four equations of boundary conditions and the above-mentioned two constitutive boundary conditions in Eq. (14), we can arrive at a system of linear equations with unknown constants $C_i\,(i = 1, 2, \cdots, 6)$ as follows:

$$\begin{pmatrix} C_{11}^{XX} & C_{12}^{XX} & C_{13}^{XX} & C_{14}^{XX} & C_{15}^{XX} & C_{16}^{XX} \\ C_{21}^{XX} & C_{22}^{XX} & C_{23}^{XX} & C_{24}^{XX} & C_{25}^{XX} & C_{26}^{XX} \\ C_{31}^{XX} & C_{32}^{XX} & C_{33}^{XX} & C_{34}^{XX} & C_{35}^{XX} & C_{36}^{XX} \\ C_{41}^{XX} & C_{42}^{XX} & C_{43}^{XX} & C_{44}^{XX} & C_{45}^{XX} & C_{46}^{XX} \\ C_{51}^{XX} & C_{52}^{XX} & C_{53}^{XX} & C_{54}^{XX} & C_{55}^{XX} & C_{56}^{XX} \\ C_{61}^{XX} & C_{62}^{XX} & C_{63}^{XX} & C_{64}^{XX} & C_{65}^{XX} & C_{66}^{XX} \end{pmatrix} \begin{pmatrix} C_1 \\ C_2 \\ C_3 \\ C_4 \\ C_5 \\ C_6 \end{pmatrix} = 0, \tag{18}$$

in which the superscript $XX$ is the boundary type.

The non-zero solution of $C_i\,(i=1,2,\cdots,6)$ requires that the determinant of the coefficient matrix $C_{mn}\,(m=1,2,\cdots,6; n=1,2,\cdots,6)$ must be zero, from which the critical buckling load of the beam can be readily calculated.

### 2.3 Effect of nonlocal heat transfer

Temperature-induced load is simplified to an equivalent external force, which is determined by using the one-dimensional nonlocal heat conduction model[41–42]

$$q_{i,i} = Q - \rho T_0 \dot{\eta}, \tag{19}$$

$$\rho\eta = (3\lambda + 2\mu)\alpha_\theta \varepsilon_{kk} + \frac{\rho c_{\mathrm{E}}}{T_0}\theta, \tag{20}$$

$$\Big(1 - \zeta^2 \frac{\partial^2}{\partial x^2}\Big) Q = -\frac{\partial}{\partial x}\Big(k\frac{\partial \theta}{\partial x}\Big), \tag{21}$$

where $q_{i,i}$ is the heat flux, $Q$ is the heat generation, $\rho$ is the mass density, $T_0$ is the initial temperature, and $\eta$ is the entropy. $\lambda$ and $\mu$ are the Lame coefficients, and $c_{\mathrm{E}}$ is the heat capacity. $\zeta$ is the nonlocal thermal parameter, and $k$ is the heat conductivity.

Let us consider the following sinusoidal heat source:

$$Q = Q_0 \sin\Big(\frac{\pi x}{2L}\Big), \tag{22}$$

where $Q_0$ is the maximum of heat generation.

Assume that the temperature at the initial end of the nanobeam would be zero, and the other end of the nanobeam is controlled by an adiabatic-like boundary. Therefore, the full boundary conditions of the nonlocal temperature field are summarized as

$$\begin{cases} \theta(x=0) = 0, \\ q(x=L) = 0. \end{cases} \tag{23}$$

Using the equations mentioned above, the temperature distribution accounting for the size effect can be given by

$$\theta = \frac{Q_0}{k}\Big(1 + \Big(\frac{\zeta}{L}\Big)^2\Big(\frac{\pi}{2}\Big)^2\Big)\Big(\frac{2L}{\pi}\Big)^2 \sin\Big(\frac{\pi x}{2L}\Big). \tag{24}$$

According to Ref. [42], the equivalent external force $N_{\mathrm{T}}$ can be expressed as

$$N_{\mathrm{T}} = \frac{1}{\int_0^L (1/EA)\,\mathrm{d}x}\int_0^L \alpha_\theta \theta\,\mathrm{d}x = b\int_{h_0}^{h_2} E(z)\,\mathrm{d}z \cdot \int_0^L \alpha_\theta \theta\,\mathrm{d}x/L. \tag{25}$$

## 3 Results and discussion

In this part, the effects of the power-law index, the nonlocal elastic parameter, and the nonlocal thermal parameter on the buckling behavior are specifically discussed via several numerical examples. The overall geometry and mechanical properties of the FG nanobeam are taken into account as[42]

$$\begin{cases} L = 10\ \mathrm{nm}, \quad b = 1\ \mathrm{nm}, \quad h = 1\ \mathrm{nm}, \\ E_{\mathrm{L}} = 70\ \mathrm{GPa}, \quad E_{\mathrm{H}} = 380\ \mathrm{GPa}, \\ k = 12.143\ \mathrm{W/(m\cdot K)}, \quad \alpha_\theta = 15.321 \times 10^{-6}\ \mathrm{K}^{-1}, \end{cases} \tag{26}$$

and the parameter of the heat source is assumed to be

$$Q_0 = \pi^5 Ik/\left(64bhL^4\alpha_\theta\right), \tag{27}$$

where $I$ is the moment of inertia.

### 3.1 Verification

First, to verify the correctness of the proposed numerical solution, a comparison between the critical buckling loads of homogeneous nanobeams predicted by the present solution (excluding the effect of temperature) and those from Barretta et al.[30] is made in Table 1. It should be explained that in Ref. [30], the negative sign represents compression, and in this study, the definition of symbol is opposite. The comparative results show that the present solution is valid.

**Table 1** Comparison of the normalized critical buckling load $P_{\rm cr} = P_{\rm cr}/P_{\text{cr-SS-classical}}$ of homogeneous nanobeams between these works and results in Ref. [30]

| Boundary | CC | CS | SS | CF | |
|---|---|---|---|---|---|
| $\alpha = 0, \xi = 0.1$ | −6.612 89 | −2.658 83 | −1.079 12 | −0.282 722 | Barretta et al.[30] |
| | 6.612 90 | 2.658 84 | 1.079 12 | 0.282 72 | Present work |
| $\alpha = 0, \xi = 0.5$ | −50.535 2 | −10.489 5 | −1.907 55 | −0.491 844 | Barretta et al.[30] |
| | 50.535 21 | 10.489 57 | 1.907 55 | 0.491 84 | Present work |

### 3.2 Parametric analysis

In this subsection, we examine the influence of the nonlocal elastic parameter $\xi$ on the critical bulking load using the stress-driven model, the power-law index being set as $\alpha = 1$. The dimensionless critical loads normalized by the results of SS beams based on the classical elasticity are described in Figs. 3(a) and 3(b). It is concluded that with the increase in the nonlocal elastic parameter, the critical buckling load grows, and for larger levels of the nonlocal elastic parameter, the discrepancies between buckling loads under different boundary edges become larger. The nonlocal elastic parameters have the greatest influence on the results of the nanobeam with the CC boundary edges. The dimensionless critical buckling load increases with the increasing nonlocal elastic parameter, indicating that the nonlocal effect of elasticity stiffens the nanobeams. However, the analysis of nanobeams based on Eringen's differential model[41] shows that the effect of the critical load is more substantial for smaller $\xi$. The softening effect conflicts with the hardening trend obtained from the experiment. The stress-driven strategy provides a good hardening prediction for the beams at the micro-nano scale. As demonstrated in Figs. 3(c) and 3(d), for different boundary edges, with an increase in $\xi$, the critical load normalized by its local counterpart increases. Furthermore, the growth rate of $P_{\rm cr}$ for CF beam is greater than that of SS beams.

Figure 4 depicts the dimensionless buckling load of FG nanobeams in terms of the power-law index $\alpha$, and those of the local elasticity theory are also provided for the sake of further comparison. With the increasing $\alpha$, the critical buckling load gradually becomes smaller, and then it tends to be stable. When the value of $\alpha$ is sufficiently large, the elastic modulus at the nanometre scale will gradually decrease and tend to $E_{\rm L}$. Through increasing the functional gradient parameter for the CC and CS beams, the decreasing trend of the critical buckling load is considerably higher than the boundary of SS and CF beams. The obtained results also indicate that for the case of the CC and CS boundary conditions, a larger axial compression load is commonly required to arrive at the buckling. When the power-law index is greater than five (i.e., $\alpha > 5$), the strengthening trend of the critical load caused by the material hardening gradually reduces.

The current FG nanobeam models based on the stress-driven integral nonlocal model can be degraded into their corresponding classical beam models. To more clearly describe the effect of functionally gradient parameters and nonlocal elastic parameters on the critical buckling load, the data from the classic model homogenous beam model and stress-driven FG nanobeam model are listed in Table 2. As is observed, the CC and CF boundary conditions have the largest and smallest dimensionless critical buckling loads, respectively, compared with those

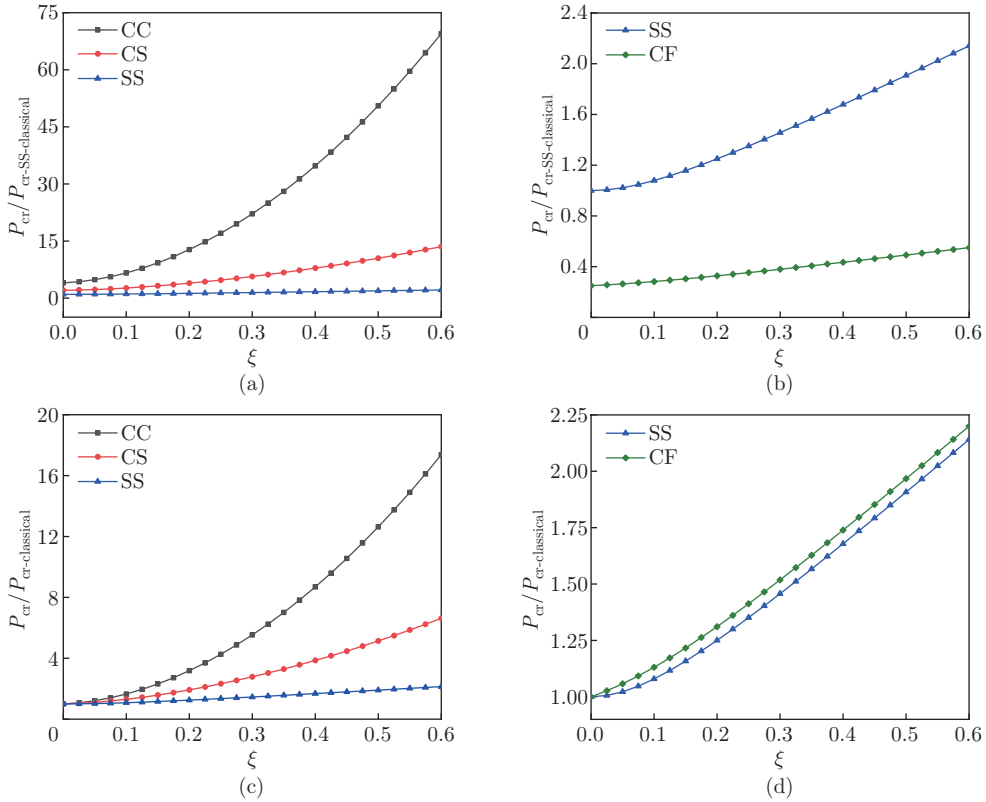


**Fig. 3** Effects of nonlocal elastic parameter $\xi$ on the critical buckling load for stress-driven nonlocal elastic nanobeams under various boundary conditions: (a) CC, CS, and SS cases normalized by the classical SS beam; (b) SS and CF cases normalized by the classical SS beam; (c) CC, CS, and SS cases normalized by the classical beam; (d) SS and CF cases normalized by the classical beam (the power-law index $\alpha = 1$) (color online)

under other boundary conditions.

By setting $Q_0 = \pi^5 Ik/(64bhL^4\alpha_\theta)$, the axial temperature distribution of the FG nanobeam is calculated and illustrated in Fig. 5. The plotted results demonstrate that the temperature increases by increasing the nonlocal thermal parameter. Figure 6 displays the proportion of the mechanical load and the equivalent axial thermal load in the normalized buckling load, where $\xi/L = 0$ and the power-law index $\alpha = 1$. When incorporating the thermal nonlocal effect, the critical mechanical load decreases. The boundary condition types have a substantial effect on the proportion of critical mechanical loads. For the case of CF boundary condition shown in Fig. 6(d), the value of normalized thermal load is greater than 1, indicating that the beam buckled without exerting any mechanical load.

Figure 7 shows the normalized critical mechanical buckling loads of FG beams for different nonlocal heat transfer parameters. By contrast, the critical mechanical buckling load value decreases when imposing a temperature load. When the nonlocal thermal parameter becomes larger, the equivalent axial thermal load grows, and further the critical mechanical buckling load decreases. This is because that the nonlocal parameter of the heat conduction affects the distribution of the temperature field in the nanobeams. Moreover, the same temperature effect has little influence on the CC boundary condition. Under the other three boundaries, the effects of parameters of the local heat transfer and nonlocal heat transfer models on the critical load can be clearly seen in Figs. 7(b)–7(d). Temperature clearly affects the obtained results

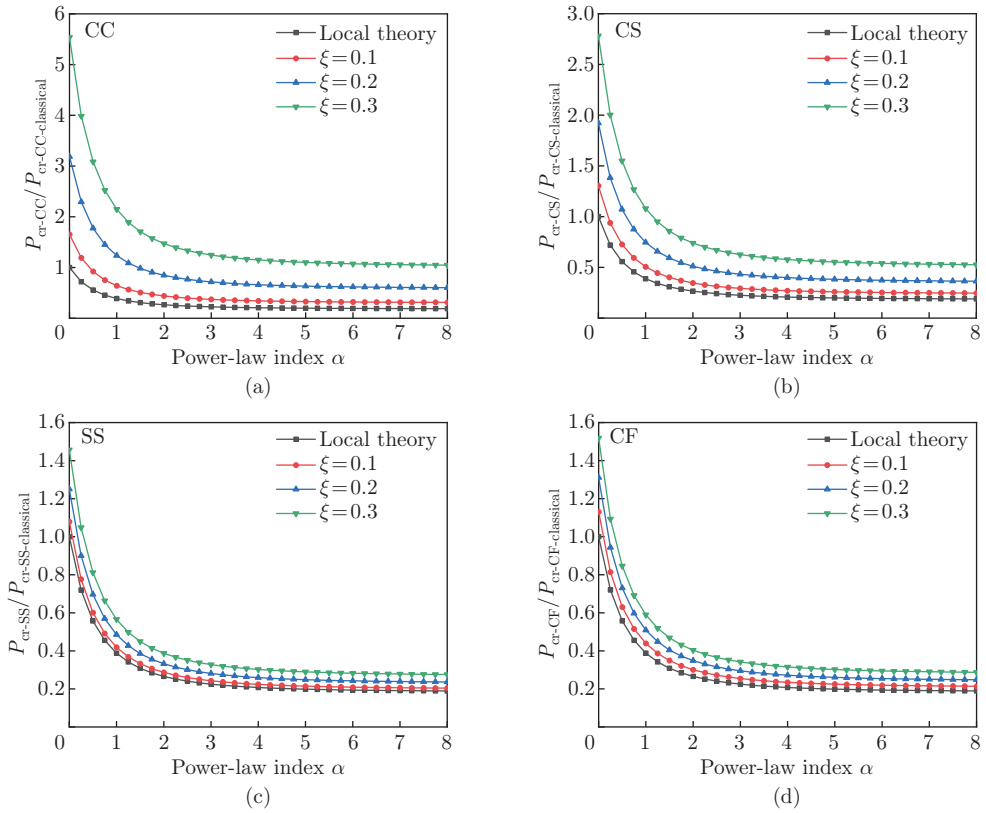


**Fig. 4** Effects of the power-law index $\alpha$ on the dimensionless critical buckling load of FG nanobeams under various boundary conditions for different elastic nonlocal parameters with $\xi = 0.1, 0.2,$ and 0.3, respectively: (a) CC; (b) CS; (c) SS; (d) CF (color online)

**Table 2** Comparison of the normalized critical bulking load $\overline{P}_{\rm cr} = 10P_{\rm cr}/(E_{\rm H}bh)$ for FG Bernoulli-Euler nanobeams with various functionally gradient indexes and different nonlocal elastic parameters

| Boundary | | Present solution | | | | | | | | |
|---|---|---|---|---|---|---|---|---|---|---|
| | | $\alpha=0$ | $\alpha=0.2$ | $\alpha=0.4$ | $\alpha=0.6$ | $\alpha=0.8$ | $\alpha=1$ | $\alpha=2$ | $\alpha=4$ | $\alpha=6$ |
| CC | $\xi=0.0$ | 0.328 98 | 0.251 21 | 0.201 56 | 0.168 12 | 0.144 68 | 0.127 69 | 0.087 44 | 0.068 27 | 0.063 79 |
| | $\xi=0.2$ | 1.048 14 | 0.800 36 | 0.642 16 | 0.535 65 | 0.460 95 | 0.406 84 | 0.278 58 | 0.217 50 | 0.203 25 |
| | $\xi=0.4$ | 2.858 39 | 2.182 69 | 1.751 25 | 1.460 78 | 1.257 07 | 1.109 51 | 0.759 73 | 0.593 17 | 0.554 30 |
| | $\xi=0.6$ | 5.714 88 | 4.363 92 | 3.501 34 | 2.920 58 | 2.513 31 | 2.218 28 | 1.518 95 | 1.185 94 | 1.108 24 |
| CS | $\xi=0.0$ | 0.167 85 | 0.128 17 | 0.102 83 | 0.085 77 | 0.073 81 | 0.065 15 | 0.044 61 | 0.034 83 | 0.032 54 |
| | $\xi=0.2$ | 0.322 65 | 0.246 37 | 0.197 67 | 0.164 89 | 0.141 89 | 0.125 23 | 0.085 75 | 0.066 95 | 0.062 56 |
| | $\xi=0.4$ | 0.647 50 | 0.494 43 | 0.396 70 | 0.330 90 | 0.284 76 | 0.251 33 | 0.172 10 | 0.134 36 | 0.125 56 |
| | $\xi=0.6$ | 1.112 12 | 0.849 21 | 0.681 36 | 0.568 34 | 0.489 09 | 0.431 67 | 0.295 58 | 0.230 78 | 0.215 66 |
| SS | $\xi=0.0$ | 0.082 24 | 0.062 80 | 0.050 39 | 0.042 03 | 0.036 17 | 0.031 92 | 0.021 86 | 0.017 06 | 0.015 94 |
| | $\xi=0.2$ | 0.102 84 | 0.078 53 | 0.063 01 | 0.052 55 | 0.045 23 | 0.039 92 | 0.027 33 | 0.021 34 | 0.019 94 |
| | $\xi=0.4$ | 0.138 05 | 0.105 42 | 0.084 58 | 0.070 55 | 0.060 71 | 0.053 58 | 0.036 69 | 0.028 64 | 0.026 77 |
| | $\xi=0.6$ | 0.176 06 | 0.134 44 | 0.107 87 | 0.089 98 | 0.077 43 | 0.068 34 | 0.046 79 | 0.036 53 | 0.034 14 |
| CF | $\xi=0.0$ | 0.020 56 | 0.015 70 | 0.012 59 | 0.010 50 | 0.009 04 | 0.007 98 | 0.005 46 | 0.004 26 | 0.003 98 |
| | $\xi=0.2$ | 0.026 95 | 0.020 58 | 0.016 51 | 0.013 77 | 0.011 85 | 0.010 46 | 0.007 16 | 0.005 59 | 0.005 22 |
| | $\xi=0.4$ | 0.035 76 | 0.027 30 | 0.021 91 | 0.018 27 | 0.015 72 | 0.013 88 | 0.009 50 | 0.007 42 | 0.006 93 |
| | $\xi=0.6$ | 0.045 23 | 0.034 53 | 0.027 71 | 0.023 11 | 0.019 89 | 0.017 55 | 0.012 02 | 0.009 38 | 0.008 77 |

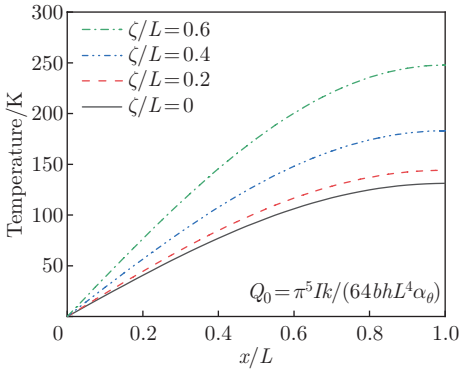


**Fig. 5** Effects of nonlocal thermal parameter $\zeta/L$ on the axial temperature distribution of the nanobeam (color online)

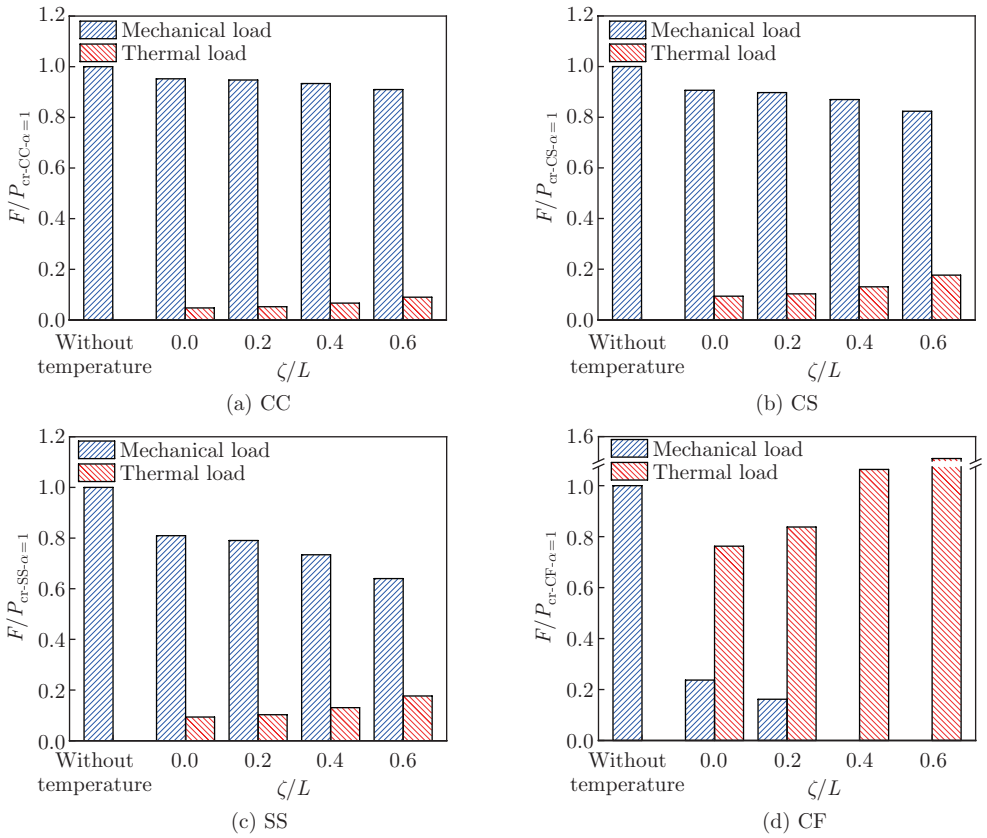


**Fig. 6** Proportions of mechanical load and thermal load in the normalized buckling load versus nonlocal thermal parameter $\zeta/L$ under various boundary conditions, (a) CC; (b) CS; (c) SS; (d) CF (the power-law index $\alpha = 1$) (color online)

in the case of CF conditions. In Fig. 7(d), the case of $F_{\rm cr} < 0$ indicates that temperature has caused the nanobeam to buckle. However, with the improvement of nonlocal elastic parameters, the material properties will gradually harden the nanobeam, effectively resisting the buckling instability caused by the thermal load. It is worth mentioning that when the temperature load is high, the beam buckling under considered boundary conditions requires serious attention.

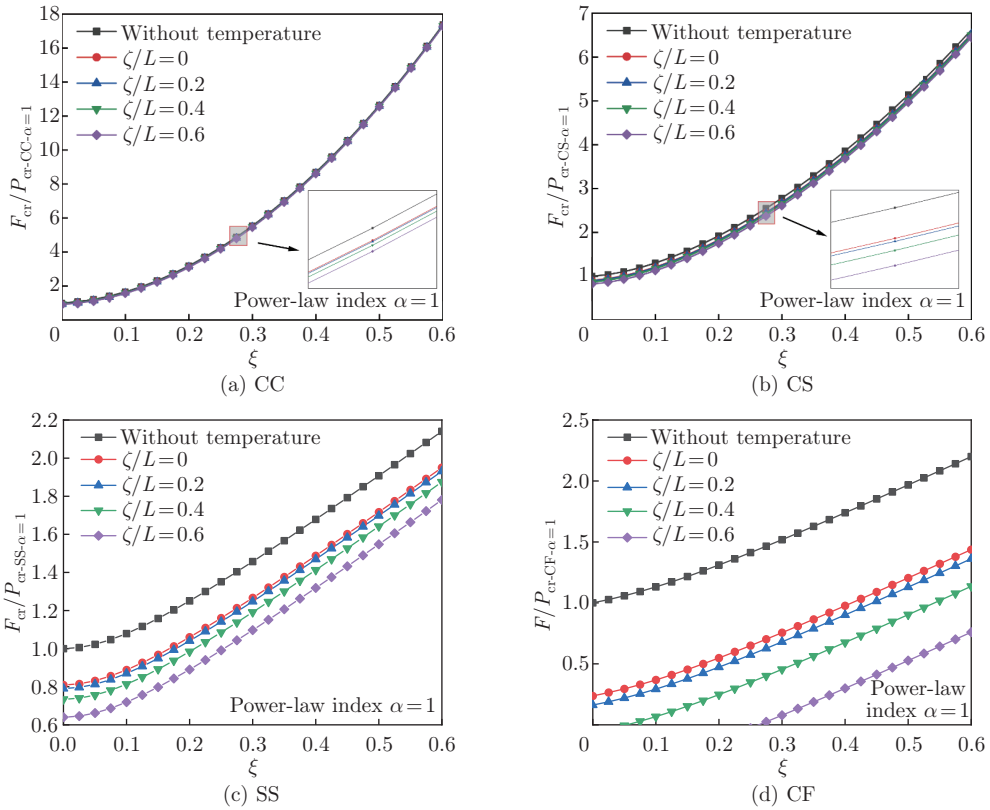


**Fig. 7** Effects of nonlocal elastic parameter $\xi$ on the normalized critical mechanical buckling loads for $\zeta/L = 0, 0.2, 0.4$, and 0.6 under various boundary conditions, (a) CC; (b) CS; (c) SS; (d) CF (power-law index $\alpha = 1$) (color online)

The plots of the normalized critical mechanical buckling load versus nonlocal thermal parameters for different power-law indexes $\alpha$ are shown in Fig. 8. The reference values denote the result from the classical beam model. The thermal temperature load causes a reduction in the critical load. The effect of the nonlocal thermal parameter on the results demonstrates an almost similar trend for all types of boundary conditions. By increasing the power-law index, the critical mechanical buckling load lessens for the same thermal nonlocal parameters. Under the CC boundary condition, the demonstrated graphs illustrate that for the same temperature field, the change of the functionally gradient index and the nonlocal parameter has little influence on the critical buckling. Nevertheless, such an effect is more noticeable for the other three end conditions, especially for the case of the CF beam. Because the temperature parameter and the functionally gradient index increase simultaneously, the nanobeam would be more unstable. In overall, the size effects of the temperature and elasticity of FG nanobeams cannot be ignored for the buckling analysis.

## 4 Conclusions

In this study, a size-dependent thermoelastic model is developed for the axial buckling analysis of FG Bernoulli-Euler beams by using the stress-driven nonlocal elasticity in conjunction with nonlocal heat conduction. The most crucial results obtained can be summarised as follows:

(I) Based on the stress-driven nonlocal elasticity model, increasing the nonlocal elastic parameter leads to a rise in the critical buckling load. With the increase in nonlocal parameters,

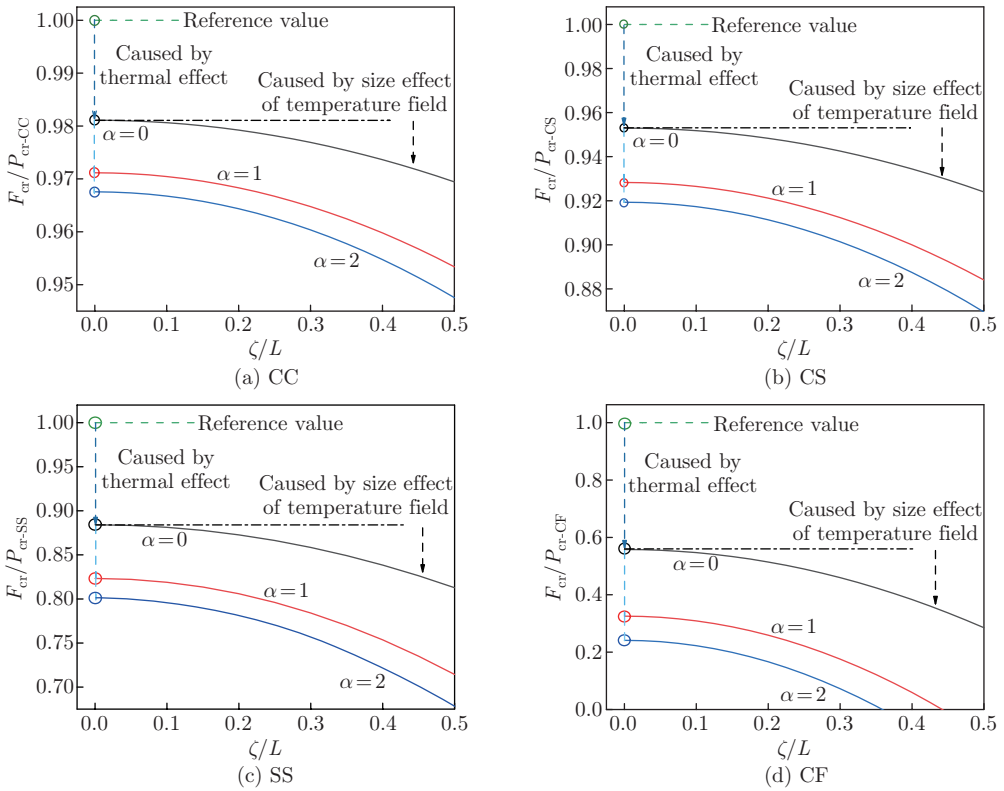


**Fig. 8** Effects of nonlocal thermal parameter $\zeta/L$ on the normalized critical mechanical buckling load with $\alpha = 0, 1$, and 2 under various boundary conditions, (a) CC; (b) CS; (c) SS; (d) CF (nonlocal elastic parameter $\xi = 0.1$) (color online)

FG nanobeams reveal different degrees of stiffening effects under four types of boundary conditions. Such an effect from large to small can be represented in order by $P_{\text{cr-CC}} > P_{\text{cr-CS}} > P_{\text{cr-SS}} > P_{\text{cr-CF}}$.

(II) For the FG beams, the critical buckling load decreases with an increase in the functionally gradient parameters, and the effect of nonlocal elastic parameter is considerably suppressed by the inclusion of the FG characteristic, particularly for $\alpha > 5$.

(III) Considering the nonlocal heat conduction model, the axial temperature distribution of nanobeams is considerably affected by the size effect. The increase in the nonlocal heat transfer parameters leads to an increase in the thermal load, severely reducing the critical buckling mechanical load. At the same temperature distribution, the CF beam tends to buckle more than other boundary conditions. The introduction of the functional gradient index requires the reconsideration of the critical buckling instability. The introduction of the functional gradient index requires the re-consideration of the critical buckling instability.

This study aims to provide a novel theoretical model for the analysis of thermomechanical buckling of FG nanobeams, and may be beneficial to further facilitating the design and usage of micro/nanoscale beams.

## References

[1] AUTUMN, K., LIANG, Y. A., HSIEH, S. T., ZESCH, W., CHAN, W. P., KENNY, T. W., FEARING, R., and FULL, R. J. Adhesive force of a single gecko foot-hair. *nature*, **405**, 681–685 (2000)

[2] KOPPERGER, E., LIST, J., MADHIRA, S., ROTHFISCHER, F., LAMB, D. C., and SIMMEL, F. C. A self-assembled nanoscale robotic arm controlled by electric fields. *Science*, **359**, 296–300 (2018)

[3] WANG, Z. L. and SONG, J. H. Piezoelectric nanogenerators based on zinc oxide nanowire arrays. *Science*, **312**, 242–246 (2006)

[4] XIANG, R., INOUE, T., ZHENG, Y. J., KUMAMOTO, A., QIAN, Y., SATO, Y., LIU, M., TANG, D. M., GOKHALE, D., GUO, J., HISAMA, K., YOTSUMOTO, S., OGAMOTO, T., ARAI, H., KOBAYASHI, Y., ZHANG, H., HOU, B., ANISIMOV, A., MARUYAMA, M., MIYATA, Y., OKADA, S., CHIASHI, S., LI, Y., KONG, J., KAUPPINEN, E. I., IKUHARA, Y., SUENAGA, K., and MARUYAMA, S. One-dimensional van der Waals heterostructures. *Science*, **367**, 537–542 (2020)

[5] PEISKER, H., MICHELS, J., and GORB, S. N. Evidence for a material gradient in the adhesive tarsal setae of the ladybird beetle Coccinella septempunctata. *Nature Communications*, **4**, 1661 (2013)

[6] ALIBARDI, L. Review: mapping proteins localized in adhesive setae of the tokay gecko and their possible influence on the mechanism of adhesion. *Protoplasma*, **255**, 1785–1797 (2018)

[7] NIX, W. D. and GAO, H. J. Indentation size effects in crystalline materials: a law for strain gradient plasticity. *Journal of the Mechanics and Physics of Solids*, **46**, 411–425 (1998)

[8] HUANG, Y., ZHANG, F., HWANG, K. C., NIX, W. D., PHARR, G. M., and FENG, G. A model of size effects in nano-indentation. *Journal of the Mechanics and Physics of Solids*, **54**, 1668–1686 (2006)

[9] ZHU, X. W. and LI, L. Closed form solution for a nonlocal strain gradient rod in tension. *International Journal of Engineering Science*, **119**, 16–28 (2017)

[10] GUO, S., HE, Y. M., LEI, J., LI, Z. K., and LIU, D. B. Individual strain gradient effect on torsional strength of electropolished microscale copper wires. *Scripta Materialia*, **130**, 124–127 (2017)

[11] GREER, J. R., OLIVER, W. C., and NIX, W. D. Size dependence of mechanical properties of gold at the micron scale in the absence of strain gradients. *Acta Materialia*, **53**, 1821–1830 (2005)

[12] LU, L., GUO, X. M., and ZHAO, J. Z. Size-dependent vibration analysis of nanobeams based on the nonlocal strain gradient theory. *International Journal of Engineering Science*, **116**, 12–24 (2017)

[13] ERINGEN, A. C. Theory of nonlocal elasticity and some applications. *Res Mechanica*, **21**, 313–342 (1987)

[14] ERINGEN, A. C. On differential equations of nonlocal elasticity and solutions of screw dislocation and surface waves. *Journal of Applied Physics*, **54**, 4703–4710 (1983)

[15] ERINGEN, A. C. Nonlocal polar elastic continua. *International Journal of Engineering Science*, **10**, 1–16 (1972)

[16] GHANNADPOUR, S. A. M., MOHAMMADI, B., and FAZILATI, J. Bending, buckling and vibration problems of nonlocal Euler beams using Ritz method. *Composite Structures*, **96**, 584–589 (2013)

[17] KHODABAKHSHI, P. and REDDY, J. N. A unified integro-differential nonlocal model. *International Journal of Engineering Science*, **95**, 60–75 (2015)

[18] SOBHY, M. and ZENKOUR, A. M. Magnetic field effect on thermomechanical buckling and vibration of viscoelastic sandwich nanobeams with CNT reinforced face sheets on a viscoelastic substrate. *Composites Part B*: *Engineering*, **154**, 492–506 (2018)

[19] LU, L., GUO, X. M., and ZHAO, J. Z. A unified nonlocal strain gradient model for nanobeams and the importance of higher order terms. *International Journal of Engineering Science*, **119**, 265–277 (2017)

[20] MIRJAVADI, S. S., RABBY, S., SHAFIEI, N., AFSHARI, B. M., and KAZEMI, M. On size-dependent free vibration and thermal buckling of axially functionally graded nanobeams in thermal environment. *Applied Physics A-Materials Science Processing*, **123**, 315 (2017)

[21] BARATI, M. R. and ZENKOUR, A. M. Investigating post-buckling of geometrically imperfect metal foam nanobeams with symmetric and asymmetric porosity distributions. *Composite Structures*, **182**, 91–98 (2017)

[22] AL-SHUJAIRI, M. and MOLLAMAHMUTOGLU, C. Buckling and free vibration analysis of functionally graded sandwich micro-beams resting on elastic foundation by using nonlocal strain gradient theory in conjunction with higher order shear theories under thermal effect. *Composites Part B*: *Engineering*, **154**, 292–312 (2018)

[23] WANG, Y. B., ZHU, X. W., and DAI, H. H. Exact solutions for the static bending of Euler-Bernoulli beams using Eringen's two-phase local/nonlocal model. *AIP Advances*, **6**, 22 (2016)

[24] ZHANG, P., QING, H., and GAO, C. F. Theoretical analysis for static bending of circular Euler-Bernoulli beam using local and Eringen's nonlocal integral mixed model. *ZAMM-Zeitschrift für Angewandte Mathematik und Mechanik*, **99**, 8 (2019)

[25] ZHANG, P., QING, H., and GAO, C. F. Analytical solutions of static bending of curved Timoshenko microbeams using Eringen's two-phase local/nonlocal integral model. *ZAMM-Zeitschrift für Angewandte Mathematik und Mechanik*, **100**, 7 (2020)

[26] ROMANO, G., BARRETTA, R., DIACO, M., and DE SCIARRA, F. M. Constitutive boundary conditions and paradoxes in nonlocal elastic nanobeams. *International Journal of Mechanical Sciences*, **121**, 151–156 (2017)

[27] FERNANDEZ-SAEZ, J., ZAERA, R., LOYA, J. A., and REDDY, J. N. Bending of Euler-Bernoulli beams using Eringen's integral formulation: a paradox resolved. *International Journal of Engineering Science*, **99**, 107–116 (2016)

[28] JIANG, P., QING, H., and GAO, C. F. Theoretical analysis on elastic buckling of nanobeams based on stress-driven nonlocal integral model. *Applied Mathematics and Mechanics* (*English Edition*), **41**(2), 207–232 (2020) https://doi.org/10.1007/s10483-020-2569-6

[29] ROMANO, G. and BARRETTA, R. Nonlocal elasticity in nanobeams: the stress-driven integral model. *International Journal of Engineering Science*, **115**, 14–27 (2017)

[30] BARRETTA, R., FABBROCINO, F., LUCIANO, R., DE SCIARRA, F. M., and RUTA, G. Buckling loads of nano-beams in stress-driven nonlocal elasticity. *Mechanics of Advanced Materials and Structures*, **27**, 869–875 (2020)

[31] BARRETTA, R., FAGHIDIAN, S. A., and LUCIANO, R. Longitudinal vibrations of nano-rods by stress-driven integral elasticity. *Mechanics of Advanced Materials and Structures*, **26**, 1307–1315 (2019)

[32] BARRETTA, R., FAGHIDIAN, S. A., and DE SCIARRA, F. M. Stress-driven nonlocal integral elasticity for axisymmetric nano-plates. *International Journal of Engineering Science*, **136**, 38–52 (2019)

[33] SEDIGHI, H. M. and MALIKAN, M. Stress-driven nonlocal elasticity for nonlinear vibration characteristics of carbon/boron-nitride hetero-nanotube subject to magneto-thermal environment. *Physica Scripta*, **95**, 055218 (2020)

[34] ZHANG, P., QING, H., and GAO, C. F. Exact solutions for bending of Timoshenko curved nanobeams made of functionally graded materials based on stress-driven nonlocal integral model. *Composite Structures*, **245**, 112362 (2020)

[35] DARBAN, H., FABBROCINO, F., FEO, L., and LUCIANO, R. Size-dependent buckling analysis of nanobeams resting on two-parameter elastic foundation through stress-driven nonlocal elasticity model. *Mechanics of Advanced Materials and Structures*, **28**, 2408–2416 (2020)

[36] BIAN, P. L. and QING, H. Torsional static and vibration analysis of functionally graded nanotube with bi-Helmholtz kernel based stress-driven nonlocal integral model. *Applied Mathematics and Mechanics* (*English Edition*), **42**(3), 425–440 (2021) https://doi.org/10.1007/s10483-021-2708-9

[37] MA, Y. B. Size-dependent thermal conductivity in nanosystems based on non-Fourier heat transfer. *Applied Physics Letters*, **101**, 211905 (2012)

[38] DONG, Y., CAO, B. Y., and GUO, Z. Y. Size dependent thermal conductivity of Si nanosystems based on phonon gas dynamics. *Physica E*: *Low-dimensional Systems and Nanostructures*, **56**, 256–262 (2014)

[39] YU, Y. J., LI, C. L., XUE, Z. N., and TIAN, X. G. The dilemma of hyperbolic heat conduction and its settlement by incorporating spatially nonlocal effect at nanoscale. *Physics Letters A*, **380**, 255–261 (2016)

[40] YU, Y. J., TIAN, X. G., and LIU, X. R. Size-dependent generalized thermoelasticity using Eringen's nonlocal model. *European Journal of Mechanics-A/Solids*, **51**, 96–106 (2015)

[41] YU, Y. J., XUE, Z. N., LI, C. L., and TIAN, X. G. Buckling of nanobeams under nonuniform temperature based on nonlocal thermoelasticity. *Composite Structures*, **146**, 108–113 (2016)

[42] LEI, J., HE, Y. M., LI, Z. K., GUO, S., and LIU, D. B. Effect of nonlocal thermoelasticity on buckling of axially functionally graded nanobeams. *Journal of Thermal Stresses*, **42**, 526–539 (2019)

[43] BARATI, M. R. and ZENKOUR, A. Forced vibration of sinusoidal FG nanobeams resting on hybrid Kerr foundation in hygro-thermal environments. *Mechanics of Advanced Materials and Structures*, **25**, 669–680 (2018)

[44] LEI, J., HE, Y. M., GUO, S., LI, Z. K., and LIU, D. B. Thermal buckling and vibration of functionally graded sinusoidal microbeams incorporating nonlinear temperature distribution using DQM. *Journal of Thermal Stresses*, **40**, 665–689 (2017)

[45] SARKAR, N. Thermoelastic responses of a finite rod due to nonlocal heat conduction. *Acta Mechanica*, **231**, 947–955 (2020)

[46] SINGH, P. and YADAVA, R. D. S. Effect of surface stress on resonance frequency of microcantilever sensors. *IEEE Sensors Journal*, **18**, 7529–7536 (2018)

[47] WU, J. Z. and ZHANG, N. H. Clamped-end effect on static detection signals of DNA-microcantilever. *Applied Mathematics and Mechanics* (*English Edition*), **42**(10), 1423–1438 (2021) https://doi.org/10.1007/s10483-021-2780-6

[48] WU, J. K. About beam (in Chinese). *Mechanics in Engineering*, **30**, 106–109 (2008)

[49] XI, Y. Y., LYU, Q., ZHANG, N. H., and WU, J. Z. Thermal-induced snap-through buckling of simply-supported functionally graded beams. *Applied Mathematics and Mechanics* (*English Edition*), **41**(12), 1821–1832 (2020) https://doi.org/10.1007/s10483-020-2696-7

## Appendix A

The nonlocal integral equation can be generally expressed as

$$f(x)=\frac{1}{2\kappa}\int_a^b \mathrm{e}^{-\frac{|x-t|}{\kappa}}\varphi(t)\,\mathrm{d}t. \tag{A1}$$

Define that

$$\begin{cases} g(x)=\displaystyle\int_a^x \mathrm{e}^{-\frac{x-t}{\kappa}}\varphi(t)\mathrm{d}t, \\ h(x)=\displaystyle\int_x^b \mathrm{e}^{-\frac{t-x}{\kappa}}\varphi(t)\mathrm{d}t, \\ f(x)=\dfrac{1}{2\kappa}(g(x)+h(x)). \end{cases} \tag{A2}$$

The first derivative in Eq. (A2) is

$$\begin{cases} g'(x)=-\dfrac{1}{\kappa}\mathrm{e}^{-\frac{x}{\kappa}}\displaystyle\int_a^x \mathrm{e}^{\frac{t}{x}}\varphi(t)\mathrm{d}t+\varphi(x), \\ h'(x)=\dfrac{1}{\kappa}\mathrm{e}^{\frac{x}{\kappa}}\displaystyle\int_x^b \mathrm{e}^{-\frac{t}{\kappa}}\varphi(t)\mathrm{d}t-\varphi(x), \\ f'(x)=\dfrac{1}{2\kappa}(g'(x)+h'(x))=-\dfrac{1}{2\kappa^2}(g(x)-h(x)). \end{cases} \tag{A3}$$

Taking the derivative of Eq. (A3) again, we get

$$f''(x)=-\frac{1}{2\kappa^2}(g'(x)-h'(x))=\frac{1}{\kappa^2}\Big(\frac{1}{2\kappa}(g(x)+h(x))-\varphi(x)\Big). \tag{A4}$$

Combining Eqs. (A2) and (A4), the equivalent differential can be obtained

$$f''(x) - \frac{1}{\kappa^2} f(x) = -\frac{1}{\kappa^2}\varphi(x). \tag{A5}$$

The constitutive boundary conditions can be derived by evaluating the above-mentioned functions at the boundary points. In view of Eq. (A2), we obtain

$$\begin{cases} g(a) = 0, \\ h(b) = 0. \end{cases} \tag{A6}$$

In the cases of $x = a$ and $x = b$, the values of $f(x)$ are stated respectively by

$$\begin{cases} f(a) = \dfrac{1}{2\kappa}(g(a) + h(a)) = \dfrac{1}{2\kappa}h(a), \\ f(b) = \dfrac{1}{2\kappa}(g(b) + h(b)) = \dfrac{1}{2\kappa}g(b). \end{cases} \tag{A7}$$

The values of $f'(x)$ at $x = a$ and $x = b$ are calculated respectively by

$$\begin{cases} f'(a) = -\dfrac{1}{2\kappa^2}(g(a) - h(a)) = \dfrac{1}{2\kappa^2}h(a), \\ f'(b) = -\dfrac{1}{2\kappa^2}(g(b) + h(b)) = -\dfrac{1}{2\kappa^2}g(b). \end{cases} \tag{A8}$$

Through mixing Eqs. (A7) and (A8), we can arrive at the following two constitutive boundary conditions:

$$\begin{cases} f'(a) - \dfrac{1}{\kappa} f(a) = 0, \\ f'(b) + \dfrac{1}{\kappa} f(b) = 0. \end{cases} \tag{A9}$$